HOLOGRAPHIC INSPECTION FOR DEBONDS IN SONAR TRANSDUCER HEAD MASS/SHROUD SUBASSEMBLIES

Cecil M. Teller

Texas Research Institute, Inc.
Austin, Texas 78733

INTRODUCTION

Holographic imaging has been successfully used to detect bubbles in the face rubber and debonds between the rubber and metal on the face and sides of the head mass and shroud of sonar transducers.[1-3] This work was done using holographic inspection equipment and techniques applied in the rubber tire industry. A considerable amount of baseline data exists for tires from which a determination of the seriousness of an observed defect can be made, but this is not yet the case for transducers. The relationship between the appearance of a holographic image and the impact of the indicated defect on the reliability and lifetime of the transducer is unknown. The basic questions are: How do debonds affect transducer lifetime? How should the fringe pattern of the holographic image be interpreted? What does the fringe pattern reveal about the size of the actual defect?

The objective of this project was therefore to quantitatively relate the parameters of a holographic image to debond dimensions and to quantify the changes in the parameters resulting from the growth of debond areas. "Debond" in this context means an unbonded area between the rubber and metal entirely contained with no channel to the outside. A bubble entirely within the rubber is a defect that also produces a holographic fringe image, but is not a "debond" and thus is not considered here.

PRINCIPLES OF HOLOGRAPHIC NDE

The fringe count in a laser holographic interference pattern is related to the surface displacement of the object under test going from an unstressed to a stressed state (see Ref. 4 for details on holographic inspection as applied to tires). Displacement can be measured with a sensitivity of $\lambda/2$, where λ is the optical wavelength of the laser source used. The overall bullseye pattern size is directly related to the physical size of the debond and inversely related to the depth of the debond, i.e., a deep debond of the same size as a shallow one would produce a smaller pattern. In the head mass/shroud inspection, stress is applied by lowering the ambient air pressure such that air or other gas trapped in a debond will expand and displace the rubber surface above it by a

small amount. This surface displacement from the unstressed state is detected with high sensitivity, typically on the order of microinches for the laser sources used. The holographic inspection technique is diagrammed in Fig. 1.

EXPERIMENTAL APPROACH

The debonds investigated were (see Fig. 2):

(a) on the face of the head mass at the rubber-aluminum interface,
(b) in the annulus between the head mass and the shroud at the rubber-aluminum (head mass) interface,
(c) in the annulus between the head mass and the shroud at the rubber-steel (shroud) interface,
(d) on the corner of the head mass at the rubber-aluminum interface, and
(e) at the interior corners of the shroud at the rubber-steel interface.

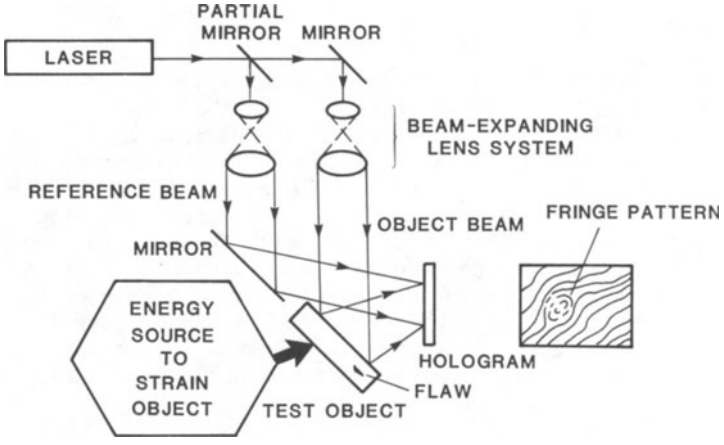

Fig. 1. Diagram of Holographic Inspection Technique

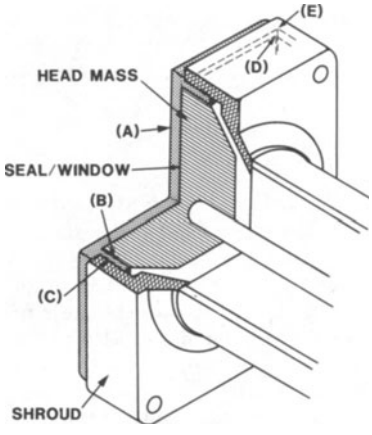

Fig. 2. Debond Locations

Specimens

Twelve head mass subassemblies (see Fig. 3) were prepared for testing. Cleaning and preparation of the surfaces for molding were done by grit blasting and vapor degreasing.

Uniroyal Vibrathane Resin No. 8090, a polyester based urethane, was used for the seal/window. This urethane rubber is transparent permitting visual confirmation of the sizes and locations of debonds. The urethane was cured with Upjohn Isonol 93 pre-polymer. Casting was carried out with a mixture of 100 parts Resin No. 8090 and 8.7 parts Isonol 93 by weight yielding 95% theoretical stoichiometry. Mixing was done at 100°C and the mixture was vacuum degassed prior to pouring. Curing was accomplished in a forced air oven at 100°C for 16 hours.

The annulus between the head mass and shroud was established by mounting the head mass on its stress rod to an aluminum plug screwed into the back of the shroud. An O-ring positioned to provide the specified depth of rubber in the annulus was used as a dam between the head mass and shroud.

All surfaces to be debonded were prepared with Thixon 416 primer/adhesive prior to casting. DuPont Vydax 525 mold release was used on the O-ring dam and the interior surfaces of the mold. After pouring, the urethane was vacuum degassed in the mold to remove any entrapped air. Shrinkage was accomodated by providing an excess of urethane at the side entry to the mold cavity. After curing, the excess material was trimmed to final dimension.

Stress relaxation tests were conducted on molded subassemblies for comparison with neoprene sealed units. The two materials compared favorably indicating successful simulation of service units. In addition, the urethane was formulated to have a hardness of approximately Shore A 60 which is typical of the neoprenes used. Hardness measurements on the cast urethane confirmed this.

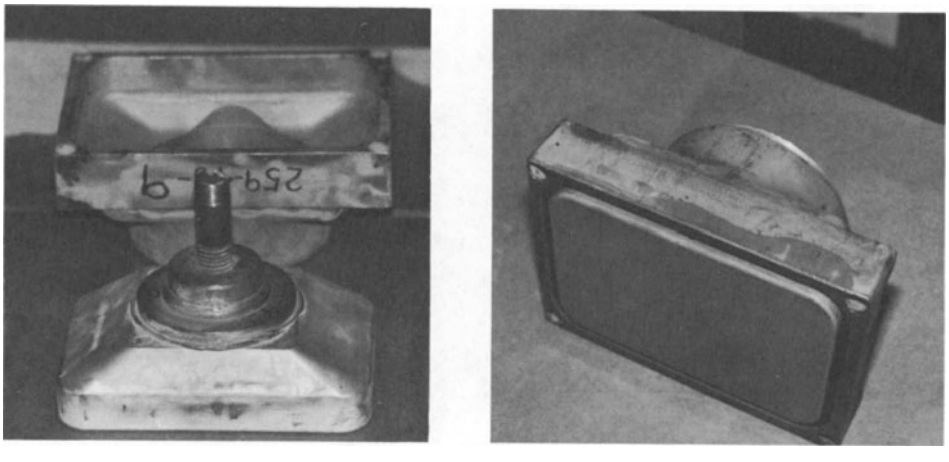

Fig. 3. Head Mass Subassembly

Debonds

The Vydax 525 mold release was used in combination with black ink to create debonds. In peel tests on small cast specimens, the debonds created in this way were confirmed to be of the size intended. The black ink provided contrast of the debond area against the metal surfaces visible through the transparent urethane rubber (see Fig. 4a).

Debonds were introduced at the five general locations described above in ten of the twelve head mass/shroud subassemblies, i.e., there were replicate specimens for each debond type. The other two subassemblies had no intentional debonds. All debonds were circular in shape and contained well within the rubber-metal interfaces with no direct air leakage paths to the outside. The face debonds ranged in size from 0.125 in. to 0.75 in. diameter. In the annulus areas the debonds ranged in size from 0.125 in. to 0.50 in. diameter since it was not possible to accommodate a 0.75 in. diameter debond.

Debond sizes were confirmed after holographic inspection by injecting a small amount of white ink with a hypodermic needle at the site of each debond (see Fig. 4b). In this way the actual size and shape of each debond could be compared directly with the programmed size and shape by visual observation through the transparent urethane. In most cases the debonds retained their intended size and shape throughout the investigation. Deviations noted were considered to be within acceptable limits.

HOLOGRAPHIC INSPECTIONS AND RESULTS

Holographic inspections were performed by Industrial Holographics, Inc. (IHI). Prior to inspection, all assemblies were coated with an opaque urethane paint so that the inspector would not know the locations of the programmed debonds. IHI also coated the assemblies with a flat white coating to improve the reflectivity of the window surfaces and applied a grid on 2 in. centers to the front face for reference purposes.

Standard holographic tire inspection techniques were employed.[5] Holographic images were acquired on each specimen at atmospheric pressure and at either three or four different vacuum levels (3, 6 and 9 or 3, 5, 7

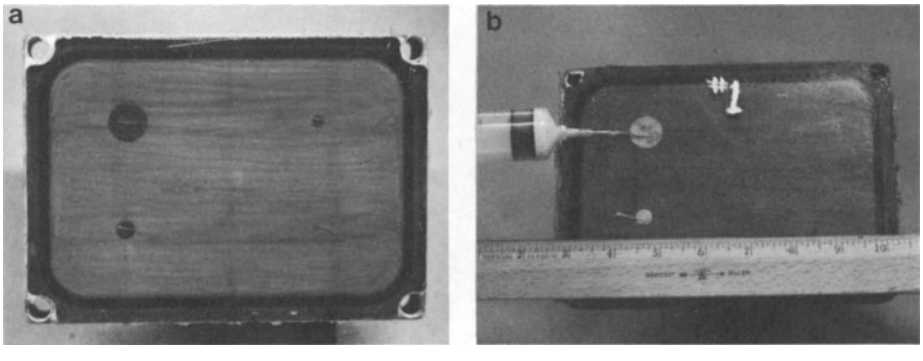

Fig. 4. Molded Head Mass Subassemblies With Induced Debonds

and 9 in. Hg). (Typically, only a 3 in. Hg vacuum level has been used in prior work.) Each specimen was allowed to return to atmospheric pressure momentarily prior to application of a higher vacuum level. For these inspections, laser pulse-up time was 2 sec, exposure time was set at 0.03 sec, and cycle time was approximately 10 min, after which the images could be examined. Photographic prints of the holographic results were produced after all inspections had been completed. Figure 5 shows example results for the face debond specimens.

Initially, the two specimens with face debonds yielded negative inspection results, i.e., no bullseye fringe patterns were detected for the programmed debonds at any vacuum level. All the other specimens (except the two with no intentional debonds) produced bullseye type fringe patterns in most locations where debonds had been introduced. Subsequently, air was injected into the face debond areas using a hypodermic needle inserted through the urethane window. This procedure "opened" the debonds and provided the necessary entrapped air upon which the holographic technique relies. Excellent fringe patterns were then obtained.

ANALYSIS

Analysis of the holographic inspection data consisted of correlating fringe counts and bullseye spot sizes with known debond dimensions at the five debond locations (see Fig. 2) and different vacuum levels.

Fringe Counts

Fringe counts were made by simply counting the number of closed, dark fringes around each known debond. For face debonds, this measurement was reasonably straightforward. For corner debonds, it was difficult to discern fringes associated with debonds from background fringes. Another difficulty was the lack of sharpness of fringes associated with some of the smaller debonds. These difficulties affect the ultimate sensitivity of the holographic technique and should be investigated more throughly.

Measurements of bullseye spot sizes were made with a Bishop 10X Optical Comparator after the fringe patterns for each debond were defined and counted. For face debonds, the diameter of the bullseye was measured at the outermost resolvable dark fringe. For annulus debonds on the sides, the minor and major axes of the generally elliptically shaped

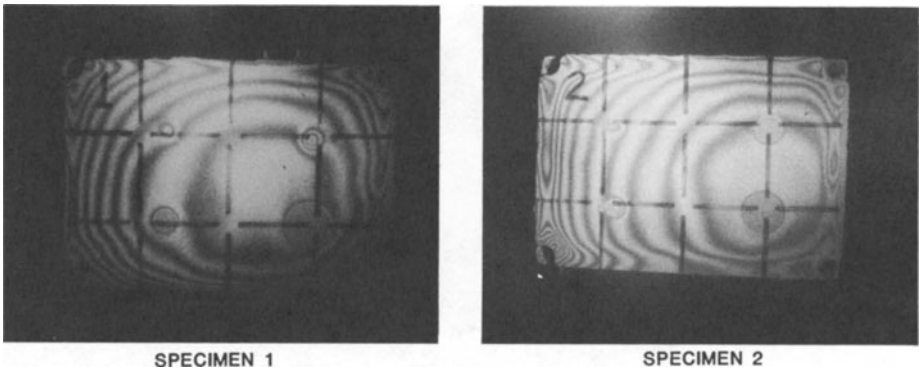

Fig. 5. Fringe Patterns - Face Debonds

bullseye were measured. For corner debonds, the length of the base of the generally triangularly shaped image was measured. Measurement accuracy was $\pm$ 0.005 in.

Correlations of dark fringe counts vs programmed debond sizes as a function of vacuum level are shown in Fig. 6. The plotted lines are best linear fits to the measured fringe counts. These data show that for all types of debonds fringe counts increase with actual debond diameter. There is also an increasing number of fringes with increasing vacuum level. Reasonably good reproducibility was observed between pairs of specimens with the same type, sizes and locations of debonds. Generally, there is separation of the curves at the different vacuum levels although overlapping does occur.

The face debonds show the largest change in fringe counts; however, this type of debond is more favorably oriented for detection by the holographic technique. The other types of debonds show less change, with the shroud side debonds showing the least change of all. In general, these data indicate that fringe count is a useful parameter for estimating actual debond size, but more data are needed to quantitatively define the reliability and confidence limits on this parameter. Also, high vacuum levels are probably not required, but different vacuum levels may be needed for optimium detection of face debonds vis-a-vis annulus debonds. The limit of sensitivity of the holographic technique appears to be approximately 0.125 in. diameter--slightly better for face debonds, slightly worse for annulus debonds.

Bullseye Spot Size

Correlations of bullseye spot sizes vs programmed debond size as a function of vacuum level are shown in Fig. 7. Again, all lines are best linear fits to the measured debond image size. For the face debonds, the relationship between indicated debond diameter and actual debond diameter at all vacuum levels investigated is shown in Fig. 7a; the line for one-to-one correlation is plotted for comparison purposes. Note that the in-

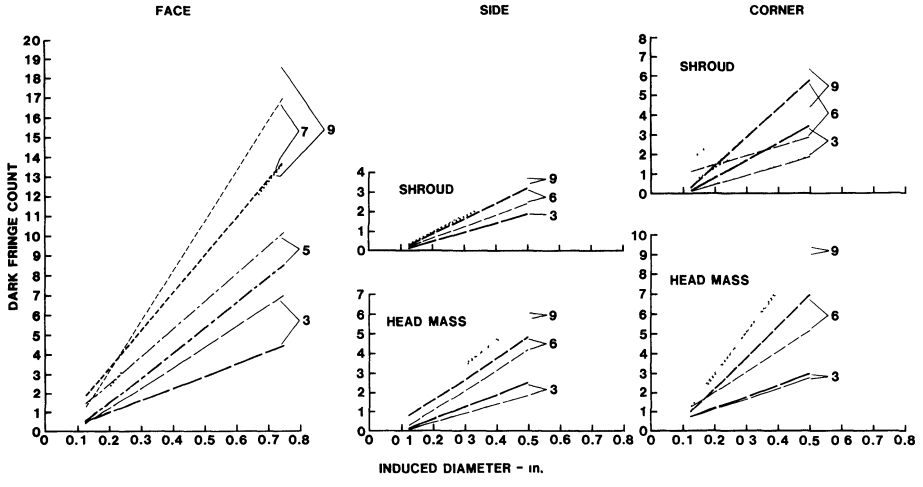

Fig. 6. Dark fringe count vs induced debond diameter; indicated debond locations. The parameter is vacuum level in inches of Mercury.

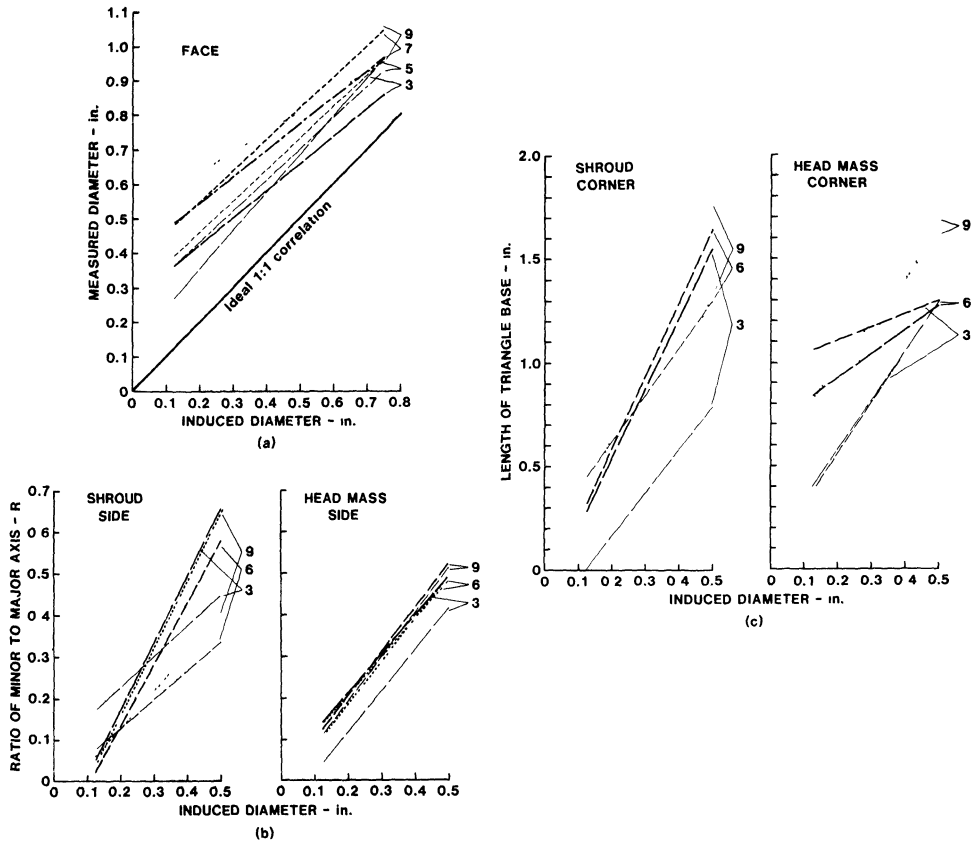

Fig. 7. Bullseye measurements vs induced debond diameter. (a) Bullseye diameter, face debonds, Location (A). (b) Ratio of bullseye axis lengths, annulus debonds, Locations (B) and (C). (c) Length of triangular bullseye base, corner debonds, Locations (D) and (E). The parameter is vacuum level in inches of Mercury.

dicated debond diameter from the image over-predicts the actual size at all vacuum levels over the entire range of debond diameters investigated. However, the correlation curves have approximately the same slope as the one-to-one correlation line and differ by a relatively constant offset which increases with vacuum level. Again, there is reasonably good repeatability between specimens at each vacuum level although overlapping does occur.

Since for debonds located on the sides of the head mass between the shroud and the head mass the bullseye patterns were elliptical, a characteristic parameter, R, defined as the ratio of the minor to major axes was chosen. This parameter produced the best correlation between the experimental data and the actual debond diameter. Figure 7b shows the correlations between R and actual debond diameter for the shroud-side and head mass-side annulus debonds. These curves show that R increases in proportion to debond size, but it is not a strong function of vacuum level. The best correlations were obtained on the head mass-side debonds since these images were somewhat less distorted by the general background fringes nearest to the edges of the rubber window.

The bullseye patterns for the debonds located at the corners of the head mass assembly were triangular with the apex of the triangle pointed toward the corner. The characteristic parameter chosen for these debonds was D, the length of the base of the triangle which runs diagonally across the corner. This parameter vs actual debond diameter is plotted in Fig. 7c for the head mass and shroud corner debonds. The values of D do not correlate well with actual debond size for the head mass corner debonds but appear to be accurate predictors of debond size for the shroud corners. The reason for this difference is not clear. Vacuum level has little effect.

CONCLUSIONS

The holographic head mass assembly inspection technique relies on the presence of trapped gas in the debond. If the debond area is weakly bonded or the debonded surfaces are in intimate contact, such that there is no trapped gas, the debond will not be detected. For conditons where the debonds contain sufficient trapped gas, analysis of the holographic image fringe count and size parameters show that both parameters have semi-quantitative relationships to actual debond size, although too few samples were analyzed to establish reliability and confidence limits. The limit of sensitivity of the technique appears to be about a 0.125 in. diameter debond. However, the measurements, especially for the very small corner debonds on the shroud side, were complicated by the presence of background fringes. Unfortunately, this type of debond is critical to transducer watertight integrity.

ACKNOWLEDGEMENTS

This work was supported by the Naval Research Laboratory, Underwater Sound Reference Detachment, Orlando, Florida, as part of the Sonar Transducer Relibility Improvement Program (STRIP). The able assistance of Mr. Shawn Arnett and Ms. Ruth Forkel and the advice and counsel of Dr. Scott Thornton, all of TRI, are greatly appreciated.

REFERENCES

1. Graham, T. S., "Production Procedures for NDT of TR-155G Molded Rubber Head Mass Assemblies Using Holographic Interferometry," BBN Tech Memo NL-072, Aug. 1982.
2. Guigli, H. J., and Graham, T. S., "Holographic Interferometry Inspection of Sixty TR-155G Head Mass Assemblies for Rubber Flaws," BBN Tech Memo NL-973, Sept. 1982.
3. Dietz, J. P., "Holographic Inspection of TR-155G and Other Head Mass Assemblies," GE Tech Memo EH-81900, 30 June 1983.
4. Grant, R. M., "Measuring Tire Quality Through the Use of Holo-Graphic and Shearographic Nondestructive Tire Testing, " Proceedings of the Annual Meeting of the American Chemical Society, 1982.
5. Grant, R. M., "Failure Analysis of Aircraft Tires as observed by Holography," Proceedings of the 4th Symposium on Non-destructive Testing of Tires, May 1978.